Journal of Modern Optics, 2014
http://dx.doi.org/10.1080/09500340.2014.899645

Taylor & Francis
Taylor & Francis Group

Experimental demonstration of Klyshko's advanced-wave picture using a coincidence-count based, camera-enabled imaging system

Reuben S. Aspden[a]*, Daniel S. Tasca[a], Andrew Forbes[b], Robert W. Boyd[a,c,d] and Miles J. Padgett[a]

[a]*SUPA, School of Physics and Astronomy, University of Glasgow, Glasgow, UK;* [b]*CSIR National Laser Centre, Pretoria, South Africa;* [c]*Department of Physics, University of Ottawa, Ottawa, ON, Canada;* [d]*Institute of Optics, University of Rochester, Rochester, NY, USA*

(*Received 10 January 2014; accepted 25 February 2014*)

The Klyshko advanced-wave picture is a well-known tool useful in the conceptualisation of parametric down-conversion (SPDC) experiments. Despite being well-known and understood, there have been few experimental demonstrations illustrating its validity. Here, we present an experimental demonstration of this picture using a time-gated camera in an image-based coincidence measurement. We show an excellent agreement between the spatial distributions as predicted by the Klyshko picture and those obtained using the SPDC photon pairs. An interesting speckle feature is present in the Klyshko predictive images due to the spatial coherence of the back-propagated beam in the multi-mode fibre. This effect can be removed by mechanically twisting the fibre, thus degrading the spatial coherence of the beam and time-averaging the speckle pattern, giving an accurate correspondence between the predictive and SPDC images.

Keywords: quantum optics; Klyshko advanced-wave picture; coincidence imaging

1. Introduction

Spatial correlations between the signal and the idler photons produced by parametric down-conversion have been the focus of many studies. The strength of the correlations in both position and momentum have been used to investigate fundamental aspects of quantum mechanics including EPR [1–3] and Bell [4] type measurements, as well as being of interest in research in quantum information and cryptographic protocols [5–8]. In 1995, it was shown that these correlations could also be used to perform "ghost imaging" [9] and "ghost diffraction" [10]. Klyshko showed that the spatial distribution of these correlations could be predicted from a simple argument based upon geometrical optics [11].

Within a standard experiment to probe spatial entanglement, a pump beam undergoes spontaneous parametric down-conversion (SPDC) in a non-linear crystal to produce signal and idler photons. These photons are correlated in position and anti-correlated in momentum. Thus, simultaneous measurements of signal and idler photons in a re-imaged plane of the crystal show strong correlations in position, whereas if measured in the far-field of the crystal their positions are anti-correlated [12]. Additional optical components or objects placed in either signal or idler beam change the strength or form of the correlations in a manner that can be calculated from the two-photon wavefunction [13,14].

Klyshko recognised that the form of these correlations could be predicted by a classical analogue [11]. Rather than using two detectors, one detector is notionally replaced by a light source. Light emitted from this source and directed back towards the down-conversion crystal is in essence the time-reversal of the parametric emission. After transmission through any optical elements, this light is reflected from the down-conversion crystal towards the other detector, i.e. the crystal is replaced by a mirror. The detected intensity at this second detector is proportional to the anticipated fourth-order correlation when the experiment is run in down-conversion mode. Importantly, one notes that in this classical analogue, the laboratory time of light emission and subsequent detection are not the same and this sequential aspect emphasises that this classical propagation from one source to the detector is a predictive tool only and most certainly not an explanation of the quantum correlations!

The analogous behaviours between the quantum and classical configurations is extensive. For example, a converging or diverging pump beam at the down-conversion crystal corresponds to making the back reflecting mirror curved, changing the direction of the pump beam corresponds to tilting the mirror [15–18]. Beyond the pump beam and back-reflecting mirror, the detailed nature of the detectors (area and numerical aperture) map directly onto the emission properties of the light source that is substituted. Despite the utility of this approach, there have been few experimental demonstrations of the equivalence between back-propagation and down-conversion.

*Corresponding author. Email: r.aspden.1@research.gla.ac.uk

In this paper, we present a full-field, 2-D, demonstration of the Klyshko advanced-wave picture in the context of a camera-enabled ghost imaging system [19]. We compare our Klyshko advanced-wave picture images with those obtained using coincidence measurements and demonstrate the equivalence between the spatial distributions in both sets of data.

2. Coincidence counts-based imaging system

To explore the equivalence between the measured spatial distribution of coincidence counts in an SPDC experiment and the Klyshko advanced-wave picture, we use the camera-enabled ghost imaging system first developed by us in reference [19] and illustrated in Figure 1(*a*). Our pump laser is a horizontally polarised, 355 nm, 120 MHz repetition rate pulsed laser used to pump a type-I phase-matched β-barium borate (BBO) crystal. This process generates two collinearly propagating, frequency-degenerate entangled photons at 710 nm which are selected using high-transmission interference filters centred on 710 nm with a bandwidth of 10 nm. The two photons are split at a beam splitter (BS) with one photon incident on a transmissive object (a skull printed on acetate, see Figure 1 and reference [19]) before being detected by a bucket detector (BD) consisting of a coupling lens, a multi-mode fibre with a core of diameter 400 μm and a single photon avalanche diode (SPAD). The signal from the SPAD is used to trigger an ICCD camera (Andor iStar). The gate width of the camera's intensifier is set by the width of the trigger pulse from the SPAD, in our case $\sim$15 ns, and the system is designed such that the correlated photon is detected during this time window. In order to account for the approximately 70 ns electronic delay in the trigger mechanism, a 22 m image-preserving, free-space delay line is introduced in the camera arm [19], shown as a dotted line in Figure 1. The correlation of the photon pairs detected in coincidence enables the spatial distribution of the object to be obtained on the camera even though none of the camera photons have been incident on the object. The object and the ICCD are located in equivalent planes relative to the BBO crystal. By switching an interchangeable lens system located between the BBO crystal and the beam splitter, these planes can be changed from the image plane (position configuration) to the far-field (momentum configuration) of the source. This procedure enables us to map either the position or momentum distributions of the photon pairs into the detection plane.

The ghost images obtained using this coincidence imaging system are shown in Figure 2(*a*). The acquisition

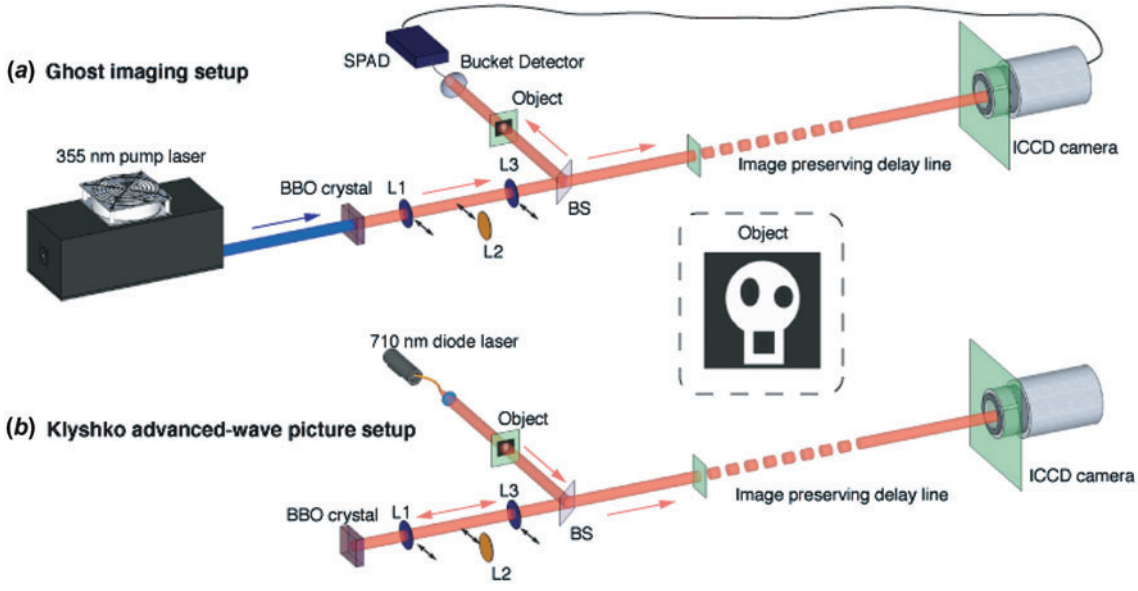

Figure 1. *(a)* Experimental set-up. Collinear down-converted photon pairs at 710 nm are generated by pumping a BBO crystal with a UV laser at 355 nm. L_1 and L_3 are 50 mm focal-length lenses used to produce an unity magnified image of the down-conversion source onto the beam splitter (BS). L_2 is a 100 mm focal-length lens used to Fourier transform the down-conversion source onto the beam splitter. The green planes are all in the far-field of the BS and this plane can be changed from near- to far-field of the BBO crystal by switching the interchangeable lens system. A 300 mm focal-length lens (not shown) is used after the beam splitter in each path to Fourier transform the down-converted fields at the beam splitter onto the planes of the object in signal arm and onto the input plane of an image-preserving delay line (DL) in idler arm. The image-preserving delay line consists of seven telescopic imaging systems, four with 1000 mm focal length lenses and three with 500 mm focal length lenses. The total length of the image-preserving delay line is 22 m. *(b)* The experimental set-up for a demonstration of Klyshko's advanced wave picture. The bucket detector is replaced by a laser diode which back-propagates through the object arm and uses the BBO crystal as a mirror, before propagating through the camera arm onto the camera. (The colour version of this figure is included in the online version of the journal.)

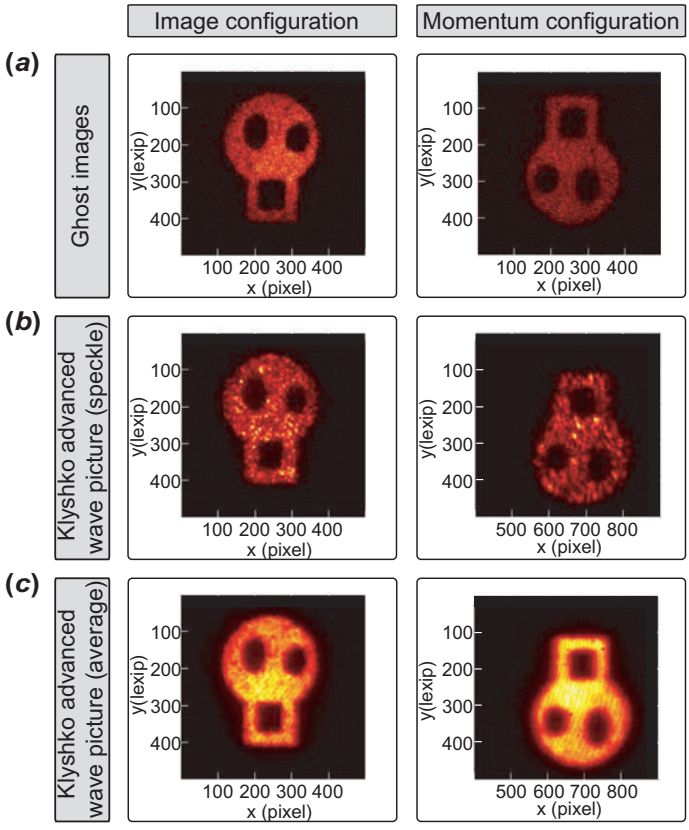

Figure 2. *(a)* Quantum ghost images obtained in the position and momentum configurations, respectively *(b)* Images obtained using the position and momentum configurations in the Klyshko advanced-wave picture set-up. The displacement of the momentum image is due to the inclination of the BBO-crystal and the speckle arises from mode-coupling in the multi-mode fibre. *(c)* Images using the position and momentum configurations in the Klyshko advanced-wave picture whilst shaking the fibre to time average the speckle. (The colour version of this figure is included in the online version of the journal.)

settings are detailed in reference [19] and we provide a brief summary here. The ghost images consist of 1800 accumulations, each of 2 s duration, during which time the intensifier fired for each single photon detection by the SPAD. Consequently, each firing of the intensifier corresponds to the detection window for a correlated single photon arriving on the ICCD. We attenuate the pump laser intensity, giving a trigger rate on the SPAD of ∼15,000 counts per second for the position configuration and ∼10,000 counts per second for the momentum configuration. This gives an average number of detected photons per accumulation of ∼70 in the position configuration and ∼40 in the momentum configuration. These count rates were chosen in order to ensure that each acquired 2 s accumulation was sparse and thus photon counting techniques could be applied [19]. The image in the momentum configuration is inverted with respect to that of the position configuration due to the momentum anti-correlations of the SPDC photons. One advantage to obtaining images in the momentum configuration over the position configuration is that the source is not imaged directly onto either the object or detection planes. This means that any defect on the facet of the crystal is not imprinted on the obtained image. Our images are detected by a 500 × 500 array of pixels which are triggered simultaneously across the full field of view of the system. This is in contrast to the standard way of obtaining such images where a single pixel detector is scanned across the detection plane [9].

3. Advanced-wave picture by means of a back-projection imaging system

As discussed in the introduction, classical optics can be used to predict the spatial distribution of coincidence counts in an SPDC set-up according to the Klyshko advanced-wave picture [11]. We implemented the Klyshko advanced-wave picture by replacing the bucket detector in our ghost imaging system with a laser diode at 710 nm as shown in Figure 1(*b*). This laser diode was coupled to the end of the multi-mode fibre and the light back-propagated through the object arm to the BBO crystal. A fraction of this back-propagated laser light was reflected at the crystal facet and redirected to the camera arm, propagating through the delay line before being recorded on the ICCD. The overall transformation undergone by the back-propagated light from the object to the ICCD is given by an unity magnification imaging

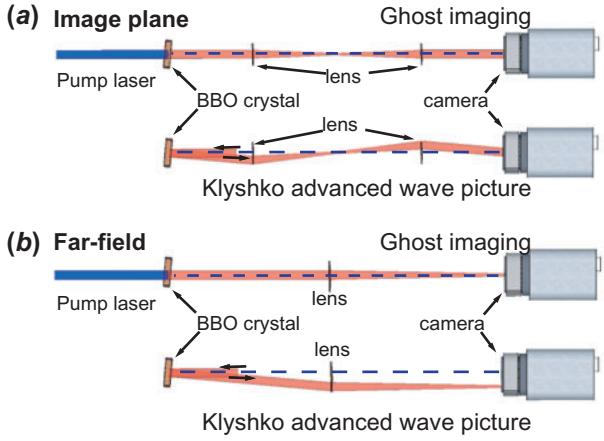

Figure 3. The effect of the phase-matching inclination of the BBO crystal on the (*a*) beam propagation through the system when imaging the crystal and (*b*) the spatial location of the back-propagated image when in the far-field of the crystal. The blue dotted line represents the optical axis. The angle of the crystal's inclination with respect to the optical axis is set by the orientation of the c-axis in the BBO crystal with respect to the facet normal and is a small angle of order one degree. (The colour version of this figure is included in the online version of the journal.)

system with $M_{PC} = -M_{MC}$ for the position and momentum configurations, respectively. The images recorded in the Klyshko picture configuration are shown in Figure 2(*b*). The spatial distribution of the images taken in the back-propagated configuration matches the corresponding ghost images.

Whereas down-converted photons display second-order coherence, the back-propagated beam only displays coherence in the first order. As a consequence of this, the propagation of the first-order coherent laser beam through the multi-mode fibre gives rise to a speckle pattern which is evident in the back-propagated images. In Figure 2(*c*), we show back-propagated images taken whilst twisting the multi-mode fibre. In this case, the mechanical bending of the fibre throughout the acquisition changes the mode-coupling conditions within the fibre and thus degrades the spatial coherence of the illumination. This results in a time averaging of the speckle pattern and we obtain smooth images comparable to the ghost images taken with the down-converted light.

We slightly tilt our BBO crystal relative to the pump beam normal in order to work in a collinear phase-matching regime. This tilt corresponds to the crystal acting as an inclined mirror to the back-propagated light, thus changing the mirror normal. In contrast, in the down-conversion configuration, this tilt does not affect the effective mirror normal, which is set by the orientation of the pump beam. In the position configuration, changing the mirror normal results in the back-propagating light arriving at the camera at a different angle to the down-converted photons, as shown in Figure 3(*a*). This small change in propagation angle does not affect the spatial distribution of the image recorded on the camera. In this case, the images recorded in the "ghost" and Klyshko's advanced picture configurations have the same intensity distribution and are registered at the same position on the camera, as shown in the left-hand column of Figure 2.

In the momentum configuration however, changing the mirror normal of the back-propagated light does result in a displacement of the back-propagated image, shown in Figure 3(*b*). The measured offset of the far-field back-propagated image on the ICCD (Figure 2(*b*) right image) due to the BBO crystal inclination is approximately 400 pixels or 5.2 mm. Using the effective focal length $f_e = 300$ mm of the Fourier system, we calculate the angle of the crystal in relation to the pump beam to be $\theta = 5.2\,\text{mm}/f_e \approx 1°$, which corresponds to the inclination angle measured with the rotation stage. A key advantage of using a camera to detect the full field of view is apparent in this context as it detects the image which would ordinarily be lost when using a scanning fibre.

Using a camera gives the ability to detect high-resolution images in both position and momentum configurations regardless of the BBO crystal orientation. This camera approach enables the utilisation of the Klyshko advanced-wave picture for the alignment of coincidence-count experiments which has not previously been possible when using scanning fibre detectors.

4. Conclusions

The Klyshko advanced-wave picture is widely conceptualised in SPDC experiments despite few experimental demonstrations of the technique. We have used a camera to show the first direct, full-field comparison between the spatial distributions of the coincidence counts in an SPDC system and those predicted using the Klyshko model. First-order interference effects give the Klyshko predictive images a speckled appearance, although this can be overcome by degrading the spatial coherence in the fibre whilst illuminating the object. There is a small displacement of the Klyshko image in the far field configuration which arises from the phase-matching angle of the crystal. We have shown that using a camera in an SPDC coincidence imaging system enables the use of the Klyshko advanced-wave picture for accurately predicting the spatial distribution of the coincidence counts. The ability to simultaneously detect over the full field of view of the system means the predictive model works without the need for any realignment between the predictive and down-conversion experiments, regardless of any phase-matching necessitated inclination of the BBO crystal.

Acknowledgements

M.J.P. would like to thank the Royal Society and the Wolfson Foundation. M.J.P and R.W.B. thank the DARPA InPho program.

R.W.B. thanks the Canada Excellence Research Chairs program. We acknowledge the financial support from the UK EPSRC.

References

[1] Leach, J.; Warburton, R.E.; Ireland, D.G.; Izdebski, F.; Barnett, S.M.; Yao, A.M.; Buller, G.S.; Padgett, M.J. *Phys. Rev. A* **2012**, *85*, 013827–013831.

[2] Edgar, M.P.; Tasca, D.S.; Izdebski, F.; Warburton, R.E.; Leach, J.; Agnew, M.; Buller, G.S.; Boyd, R.W.; Padgett, M.J. *Nat. Commun.* **2012**, *3*, 984–100.

[3] Howell, J.C.; Bennink, R.S.; Bentley, S.J.; Boyd, R.W. *Phys. Rev. Lett.* **2004**, *92*, 210403–210407.

[4] Yarnall, T.; Abouraddy, A.F.; Saleh, B.E.A.; Teich, M.C. *Phys. Rev. Lett.* **2007**, *99*, 170408–170412.

[5] Di Giuseppe, G.; Martin, L.; Perez-Leija, A.; Keil, R.; Dreisow, F.; Nolte, S.; Szameit, A.; Abouraddy, A.F.; Christodoulides, D.N.; Saleh, B.E.A. *Phys. Rev. Lett.* **2013**, *110*, 150503–150508.

[6] Almeida, M.P.; Walborn, S.P.; Ribeiro, P.H.S. *Phys. Rev. A* **2005**, *72*, 022313–022320.

[7] O'Sullivan-Hale, M.N.; Khan, I.A.; Boyd, R.W.; Howell, J.C. *Phys. Rev. Lett.* **2005**, *94*, 220501–220505.

[8] Walborn, S.P.; Lemelle, D.S.; Almeida, M.P.; Souto Ribeiro, P.H. *Phys. Rev. Lett.* **2006**, *96*, 090501–090505.

[9] Pittman, T.B.; Shih, Y.H.; Strekalov, D.V.; Sergienko, A.V. *Phys. Rev. A* **1995**, *52*, R3429–R3432.

[10] Strekalov, D.V.; Sergienko, A.V.; Klyshko, D.N.; Shih, Y.H. *Phys. Rev. Lett.* **1995**, *74*, 3600–3603.

[11] Klyshko, D.N. *Uspekhi Fizicheskikh Nauk* **1988**, *154*, 133–152.

[12] Walborn, S.P.; Monken, C.H.; Padua, S.; Souto Ribeiro, P.H. *Phys. Rep.* **2010**, *495*, 87–139.

[13] Tasca, D.S.; Walborn, S.P.; Souto Ribeiro, P.H.; Toscano, F.; Pellat-Finet, P. *Phys. Rev. A* **2009**, *79*, 033801–033810.

[14] Kang, Y.; Cho, K.; Noh, J.; Vitullo, D.L.P.; Leary, C.; Raymer, M.G. *Opt. Express* **2010**, *18*, 1217–1233.

[15] Pittman, T.B.; Strekalov, D.V.; Klyshko, D.N.; Rubin, M.H.; Sergienko, A.V.; Shih, Y.H. *Phys. Rev. A* **1996**, *53*, 2804–2815.

[16] Monken, C.H.; Ribeiro, P.H.S.; Padua, S. *Phys. Rev. A* **1998**, *57*, 3123–3126.

[17] Oemrawsingh, S.S.R.; de Jong, J.A.; Ma, X.; Aiello, A.; Eliel, E.R.; 't Hooft, G.W.; Woerdman, J.P. *Phys. Rev. A* **2006**, *73*, 032339–032346.

[18] McLaren, M.; Romero, J.; Padgett, M.J.; Roux, F.S.; Forbes, A. *Phys. Rev. A* **2013**, *88*, 033818–033826.

[19] Aspden, R.S.; Tasca, D.S.; Boyd, R.W.; Padgett, M.J. *New J. Phys.* **2013**, *15*, 073032–073043.